FULL PAPER

Optoelectronic Artificial Synapses

ADVANCED
FUNCTIONAL
MATERIALS
www.afm-journal.d

Photoelectric Synaptic Plasticity Realized by 2D Perovskite

Yilin Sun, Liu Qian, Dan Xie,* Yuxuan Lin, Mengxing Sun, Weiwei Li, Liming Ding,* Tianling Ren, and Tomás Palacios

Recently, several light-stimulated artificial synaptic devices have been proposed to mimic photonic synaptic plasticity for neuromorphic computing. Here, the photoelectric synaptic plasticity based on 2D lead-free perovskite ($(PEA)_2SnI_4$) is demonstrated. The devices show a photocurrent activation in response to a light stimulus in a neuron-like way and exhibit several essential synaptic functions such as short-term plasticity (STP) and long-term plasticity (LTP) as well as their transmission based on spike frequency control. The strength of synaptic connectivity can be effectively modulated by the duration, irradiance, and wavelength of light spikes. The ternary structure of $(PEA)_2SnI_4$ causes it to possess varied photoelectric properties by composition control, which enhances the complexity and freedoms required by neuromorphic computing. The physical mechanisms of the memory effect are attributed to two distinct lifetimes of photogenerated carrier trapping/detrapping processes modulated by controlling the proportion of Sn vacancies. This work demonstrates the great potential of $(PEA)_2SnI_4$ as a platform to develop future multifunctional artificial neuromorphic systems.

1. Introduction

The human brain works as a control center of the nervous system and is composed of $\approx 10^{11}$ neurons connected by $\approx 10^{15}$ synapses, which results in many unique computational capabilities such as a high degree of parallelism, low power consumption, and fault-tolerance.[1] The parallel information processing by the human brain is much more efficient than that of modern digital computers based on von Neumann's architecture with the memory and processor physically separated.[2] Inspired by these powerful signal processing abilities of the human brain, synapse-like artificial devices have been proposed to mimic the processing and transmission of signals in a human brain.[3] In a biological neural system, synapses refer to the junctions between adjacent neurons specialized for signal transmission.[4] Notably, the most significant property of synapses is their plasticity, which represents the changes in synaptic strength and is responsible for learning and memorization.[5] Recently, numerous efforts have been made to explore electric-driven synaptic devices such as two-terminal memristors[6] and three-terminal synaptic transistors based on ZnO, graphene, and carbon nanotubes.[7–9] In addition, several artificial synaptic transistors based on conjugated polymers have been proposed for neuromorphic computing.[10–12] These works indicate the great research interest and the urgent demands on the new device architecture and material system for artificial synapses.

In spite of such a great technological advancement, current synaptic devices composed of pure electronic components could not implement the functions of sensory cells such as ocular, olfactory, or auditory cells in biological nervous systems,[13,14] and the lack of sensing components specifically designed for neuromorphic circuits may give rise to undesirable hardware redundancy and system latency.[15] Furthermore, true synapse plasticity requires the ability to deal with multivariate connectivity strengths,[16] whereas electrically stimulated synaptic devices are probably incapable of further emulating the complex activities of real organisms due to a fixed coupling coefficient[15] and the speed of neural operation in electrically stimulated devices can be limited due to the bandwidth–connection-density tradeoff.[17] Therefore, new multifunctional synaptic devices, which could respond to various stimuli in addition to electrical stimuli and process multiple inputs in parallel in the same way biological neurons do, are urgently needed.

Compared with conventional electrically stimulated devices, a synaptic device responding to light stimuli may be advantageous in terms of wider bandwidth, low crosstalk, and better scalability, which may contribute to an enhanced computational speed of neural networks.[17–19] Therefore, seeking new

Y. Sun, Prof. D. Xie, M. Sun, W. Li, Prof. T. Ren
Institute of Microelectronics
Tsinghua National Laboratory for Information Science and Technology (TNList)
Tsinghua University
Beijing 100084, China
E-mail: xiedan@tsinghua.edu.cn
Y. Sun, Y. Lin, Prof. T. Palacios
Department of Electrical Engineering and Computer Science
& Microsystems Technology Laboratories (MTL)
Massachusetts Institute of Technology
77 Massachusetts Avenue, Cambridge, MA 02139, USA
Dr. L. Qian, Prof. L. Ding
Center for Excellence in Nanoscience
Key Laboratory of Nanosystem and Hierarchical Fabrication (CAS)
National Center for Nanoscience and Technology
Beijing 100190, China
E-mail: ding@nanoctr.cn

functional elements and architectural designs that emulate biological synapses in response to light stimuli with high sensitivity is of great importance. Recently, several works have demonstrated the great potential of light-stimulated synaptic devices for neuromorphic computing.[15,17,20,21] However, the origins of light-stimulated synaptic plasticity reported in such works have been widely attributed to the defects located at the surface or interface between functional layers, which may not be stable and controllable. Furthermore, the fixed device structure or material composition could not satisfy the requirement for freedom, which means that the variables act or work without constraints, as required by complicated neuromorphic computing. Here, we propose a synaptic photoconductor based on 2D layered perovskite, which can be regarded as the derivatives of conventional 3D perovskites by replacing small methylammonium (MA+) with large ammonium cations, such as phenylethylammonium (PEA+). This kind of material has been considered as a promising candidate for either artificial photosensory cells or optoelectronic implementations of neuromorphic computing, for three reasons. First, organic–inorganic hybrid perovskites have emerged as efficient photosensitive materials with large light absorption coefficients, and long carrier lifetimes and diffusion lengths.[22,23] In the past few years, a wide range of optoelectronic devices based on perovskites such as solar cells,[24] light emitting diodes,[25] and photodetectors[26] have been demonstrated. Second, perovskites have been found to be promising in resistive memory devices, where ionic migration and diffusion have been employed to realize artificial synapses.[27] Third, perovskite-based photomemories have also been demonstrated with reproducible data writing/erasing cycles.[28] However, the distinctive feature separating 2D perovskite from other photosensitive materials is the easily modulated optical and electrical properties obtained by modifying its composition during the synthesis process.[29–31] In this way, 2D perovskite via a one-step solution processing method can offer a necessary degree of freedom by chemical engineering and satisfy the complexity required by neuromorphic computing.

As a proof-of-concept demonstration, we fabricated photoconductors based on a 2D layered perovskite (($PEA)_2SnI_4$) to mimic synaptic behaviors under light stimuli. In such artificial synapse, synaptic plasticity such as paired-pulse facilitation (PPF) in response to light stimuli was implemented. The conversion between short-term plasticity (STP) and long-term plasticity (LTP), which have been considered as the foundation of memory function in the human brain, has been achieved by modulating the frequency and numbers of light spikes. Moreover, Sn vacancy-dominant memory characteristics in $(PEA)_2SnI_4$ have been demonstrated to highlight the great potential of 2D perovskite as a functional layer in light-stimulated synaptic devices.

2. Results and Discussion

A 3D schematic of a synaptic device based on $(PEA)_2SnI_4$ is illustrated in **Figure 1**a, and the optical images of such a device with a channel length of ≈7 µm and width of ≈50 µm can be found in Figure S1 of the Supporting Information. The inset in the top left corner shows the crystal structure of $(PEA)_2SnI_4$,

where the inorganic layers comprise a single sheet of corner sharing metal-halide octahedral, sandwiching layers of PEA+ cations. The X-ray diffraction (XRD) patterns of $(PEA)_2SnI_4$ film exhibit peaks at 5.4°, 10.8°, 16.2°, 21.8°, 27.4°, 33.0°, and 38.6°, which can be ascribed to the diffractions from (0 0 l) (l = 2, 4, 6, 8, 10, 14) planes of the crystal (Figure S2, Supporting Information), confirming its 2D crystalline structure. The top view scanning electron microscope (SEM) image of the $(PEA)_2SnI_4$ film indicates a smooth surface with plate-like crystals (Figure S3, Supporting Information). These results confirm the formation of a $(PEA)_2SnI_4$ crystal with a 2D layered structure.[28] The absorption spectrum of $(PEA)_2SnI_4$ film indicates a light absorption edge at the wavelengths of ≈650 nm as shown in Figure 1b. To characterize the photoelectric performance of $(PEA)_2SnI_4$, the temporal response under different wavelengths with the same light irradiance has been investigated (Figure S4, Supporting Information). The photocurrents extracted from Figure S4 of the Supporting Information have been labeled with stars in Figure 1b, indicating a higher photoresponsivity at 470 nm and a good consistency with the absorption spectrum. Therefore, the 470 nm light spike is selected as the input signal to stimulate the 2D perovskite-based artificial synaptic. The conductance change of the perovskite in response to the 470 nm presynapse light stimuli, defined as postsynapse current (PSC), is used as the output signal to emulate the strength of the synaptic connection between neurons, i.e., synaptic weight as shown in Figure 1c.[32]

As illustrated in Figure 1d, the change of PSC (ΔPSC) increases under the light stimuli, which corresponds to the excitatory postsynaptic current and indicates the potentiation of the synaptic strength.[33,34] Then, the PSC quickly returns to its initial value when the light stimuli are removed, which represents a typical STP behavior observed in biological synapses.[35] In biological synapses, the STP can be converted into LTP inside the cerebral cortex via a process called consolidation when maintenance rehearsal of the stimulation is applied.[36] In neuroscience, STP and LTP have been seen as the basic learning and memory mechanisms. Figure 1e,f illustrates the conversion from STP to LTP by applying light spikes with different frequencies at the same light irradiance of 11.6 µW cm⁻². After a series of light spikes with a duration of 20 ms and a period of 1 s is applied, the PSC quickly returns to its initial value as ΔPSC equals 0. However, if the high-frequency (20 Hz) light spikes with the same irradiance and duration are applied, which can be seen as maintenance rehearsal, the ΔPSC will slowly decay after the end of the light spikes, indicating an LTP behavior (Figure 1f). Another attempt to achieve such conversion between the STP and the LTP is by applying the same number of light spikes with different frequencies (Figure S5, Supporting Information), where similar STP/LTP conversion behaviors were observed. These results demonstrate the frequency-dependent synaptic plasticity, where the synaptic strength can be directly modulated by the repeated training process. In addition, the ΔPSCs triggered by a series of light spikes under different voltage biases ranging from 0.5 to 2 V have been investigated (Figure S6, Supporting Information), which demonstrates the operation of 2D perovskite-based synaptic devices at a lower voltage bias.
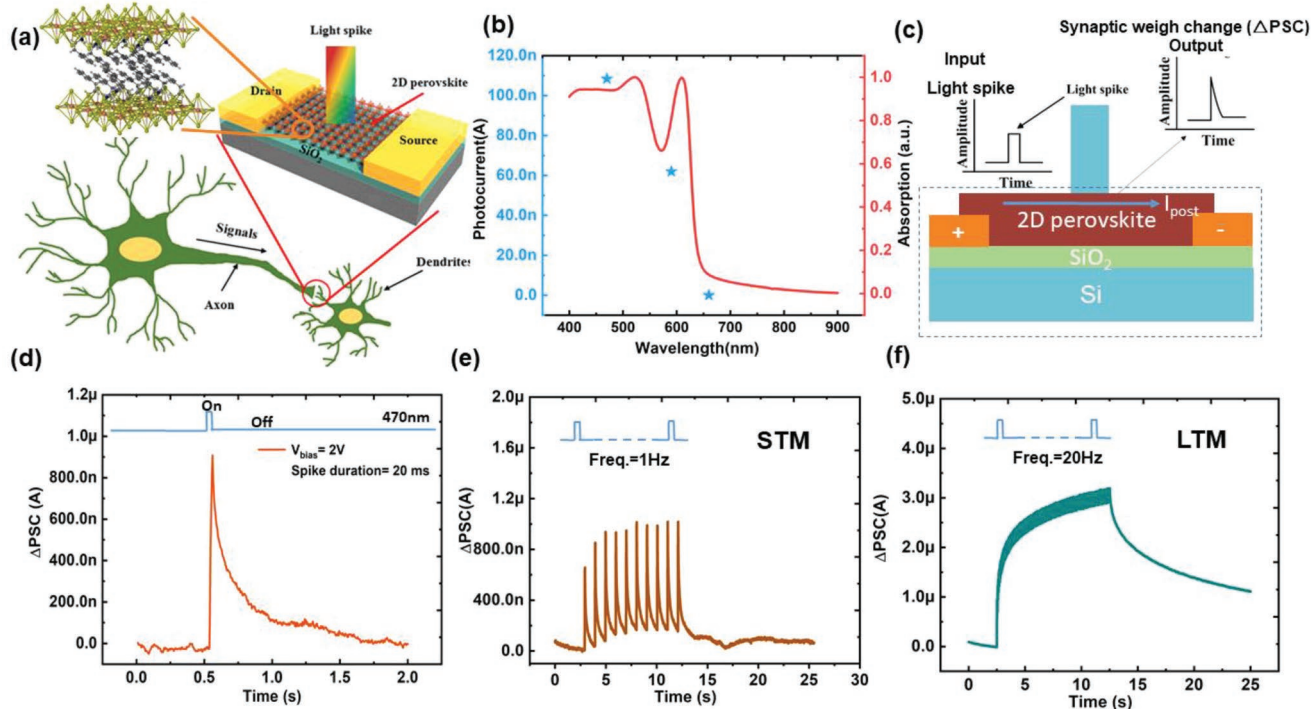
Figure 1. a) Schematic of a biological synapse and the signal transmission process from axons to dendrites. The synaptic devices shown in the top right corner resemble such a signal transmission process, with light spikes as the input signals and current spikes in the $(PEA)_2SnI_4$ layer as the output signals. The inset in the top left corner is the crystal structure of 2D layered $(C_6H_5CH_2CH_2NH_3)_2SnI_4$ (orange balls, tin atoms; yellow balls, iodine atoms; blue balls, nitrogen atoms; dark grey balls, carbon atoms; light grey balls, hydrogen atoms). b) The UV–vis absorption spectrum of a $(PEA)_2SnI_4$ film (red line) and the photocurrents of $(PEA)_2SnI_4$-based photoconductor under illumination at wavelengths of 470, 590, and 660 nm at the same irradiance of 5 µW cm^{-2}, respectively (blue stars). c) Cross-sectional illustration of the artificial synaptic devices. The insets are examples of the input light spikes and the output PSC. d) The change of PSC (ΔPSC) triggered by a light spike (wavelength = 470 nm, duration time = 20 ms and power density = 11.6 µW cm^{-2}) under a bias voltage (V_{bias}) of 2 V. The emulation of e) STP (duration = 20 ms, frequency = 1 Hz) and f) LTP (duration = 20 ms, frequency = 20 Hz) behaviors by frequency-varied light stimuli.

To discuss the learning mechanism in our artificial synapse, pairedpulse facilitation (PPF) of our artificial synapse is investigated, which is considered the basic operation of the temporal information encoding of auditory or visual signals.[15] **Figure 2a** shows a schematic of two adjacent neurons with a synapse in a biological nervous system. In a biological synapse, PPF indicates a synaptic process where the release of the neurotransmitter can be enhanced due to the activation by two closely spaced stimuli. Here, a pair of light spike (11.6 µW cm^{-2}, 20 ms) with a time delay (Δt) of 1s is applied as shown in the inset of Figure 2a. From Figure 2b, it can be clearly seen that the ΔPSC triggered by the second light spike is larger than that triggered by the first one. When Δt is smaller than the recombination time of the photogenerated carriers, the ΔPSC triggered by the second light spike can be enhanced by the residual photogenerated carriers excited by the first light spike. To further evaluate the PPF properties of our artificial synaptic devices, the PPF index is introduced as PPF = $A_2/A_1 \times 100\%$, where A_2 and A_1 represent the amplitude of ΔPSC triggered by the second light spike and the first light spike, respectively. The PPF index is plotted as a function of Δt in Figure 2c, which indicates a maximum PPF index of 129.7% when $\Delta t = 50$ ms and an exponential decay of the PPF index with the increase in Δt. Such a decay can reflect a learning pattern associated with frequently repeated training spikes in biological synapses.[12]

Figure 2d represents the ΔPSC response to a train of 10 light spikes with a spike duration of 20 ms at a frequency of 20 Hz. The ΔPSC is improved significantly and the memory retention time is also extended compared with that triggered by a single light spike, revealing a short-term learning and memory effect by repeated presynaptic stimulations. Figure 2e shows the relationship between ΔPSC and number of light spikes, indicating a nonlinear response of our synaptic devices to the number of light spikes. Furthermore, the PSC gain, defined as A_{10}/A_1, is used to characterize such a strengthening induced by a train of light spikes with different frequencies, where A_1 and A_{10} represent the peak values of ΔPSC triggered by the first and the tenth light spikes, respectively (Figure 2d). The PSC gain is plotted as a function of the frequency in each spike train as shown in Figure 2f. When the spike frequency increases, the EPSC gain is enhanced from 1.29 (1 Hz) to 2.02 (20 Hz). Such behaviors reveal that our synaptic device can work as a dynamic high-pass filter for information transmission.[7,37] Based on the results, the high-repetition training spikes can contribute to the improvement of learning in our artificial synapse. This learning and memory process can be attributed to the slow recombination of photogenerated carriers, which strengthens the photoresponse activated by the following spike. The frequency-dependent synaptic transmission has been found to be one of the fundamental mechanisms that are the principle of many
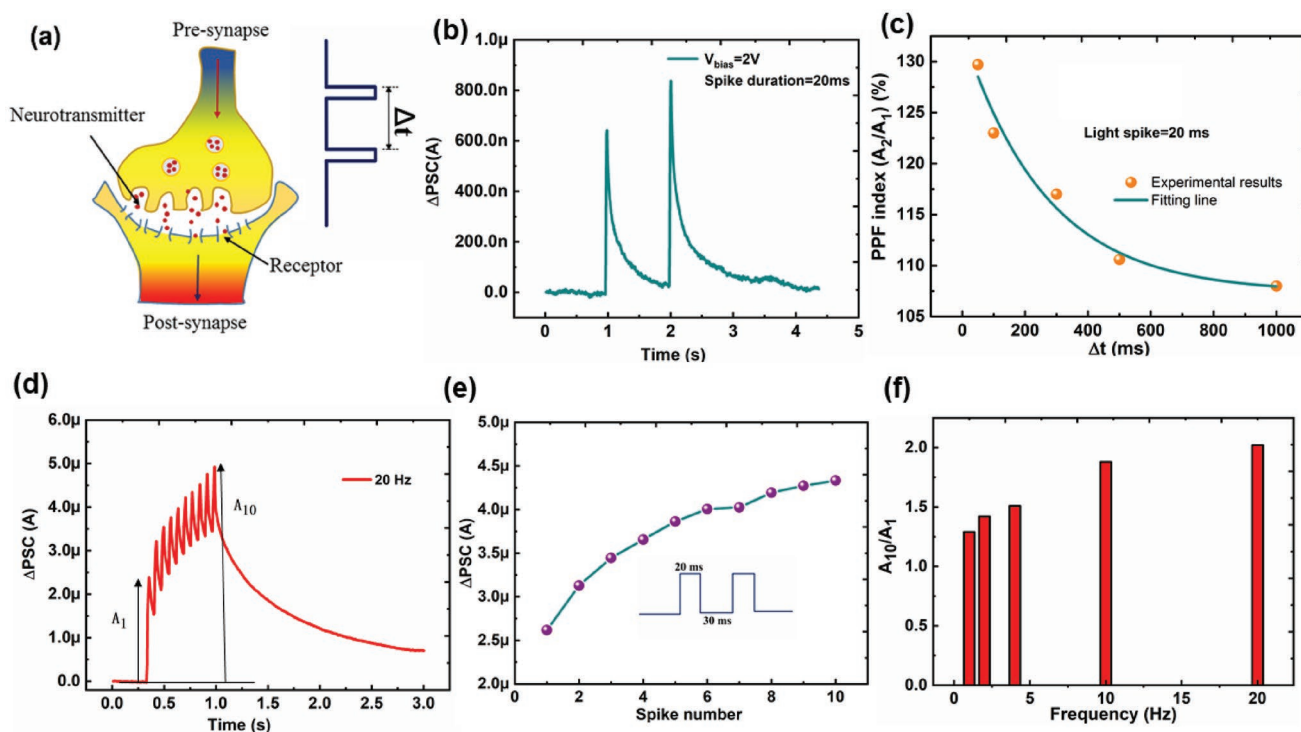
Figure 2. a) Schematic of a biological synapse triggered by a pair of presynaptic action potentials with the time interval (Δt). b) The ΔPSC triggered by a pair of presynaptic light spikes with an interval of 1 s. A_1 and A_2 represent the amplitudes of the first and second ΔPSCs, respectively. c) PPF index defined as A_2/A_1 is plotted as a function of light spike interval time Δt. The fitting line indicates that the PPF index exponentially decreases with the increase of Δt. d) The ΔPSC triggered by a train of 10 light spikes (20 ms, 20 Hz) obtained from another similar device with a larger width of approximately 150 µm. A_1 and A_{10} represent the amplitudes of the first and tenth ΔPSCs, respectively. e) The ΔPSC plotted as a function of the spike number; f) The PSC gain (A_{10}/A_1) plotted as a function of the light spike frequency.

neural computations such as orientation detection and sound-source localization.[38,39]

Another important key property of biological synapse is the adaptable response to the change of external stimuli, especially for the visual sense, where the neurons need to adjust their response to dramatically changing stimuli by changing the light exposure dosage.[40] If the photoresponse is easily saturated by a stronger exposure or not sensitive enough to a weaker exposure, it may be difficult to make an accurate recognition. Such a feature can be captured by the response of an artificial synapse to different spike durations and the light irradiances. The ΔPSC response of our device against a light spike train with different spike durations is investigated as shown in **Figure 3**a. The amplitude of ΔPSC has been extracted as a function of the spike duration shown in Figure 3b. It can be clearly seen that a longer spike duration can trigger a larger ΔPSC and a longer memory retention time. In addition to the strong spike frequency and duration dependences, we also found efficient modulations of light irradiances on the strength of synaptic behaviors. A train of light spikes with the same duration but different irradiances ranging from 5.1 to 49.1 µW cm^{-2} is applied onto the device (Figure 3c). From Figure 3d, it can be clearly seen that the ΔPSC linearly increases with the increase in the light spike irradiance. The linear relations between ΔPSC and the spike duration as well as the light irradiance indicate that our artificial synapse can dynamically respond to the light spike, which is necessary for most biological photosensors

to obtain accurate performances with different functions in information processing.[37]

In addition, the controllable photoelectric properties of perovskite, especially for wavelength selectivity, can make it respond to varied light spikes with different wavelengths, which shows the great potential for synapse-based computing.[15] Figure S7 of the Supporting Information shows the wavelength-dependent transient photoresponse of 2D perovskite to the light stimulation. Blue ($\lambda = 460–470$ nm), green ($\lambda = 520–530$ nm), red ($\lambda = 620–630$ nm), and white light-emitting diodes (LEDs) are used as light sources to evaluate the characteristics. From the results, the highest ΔPSCs are induced by the white and blue LEDs and the smallest ΔPSC is induced by red LEDs. This is consistent with the absorption spectrum of $(PEA)_2SnI_4$ film shown in Figure 1b. The light-stimulated synaptic devices based on 2D perovskite show much higher selectivity than electric stimuli, which may be used to trigger some special neurons in biological systems. Compared with other photoelectric materials, the photoelectric properties of our 2D perovskite can be easily modulated by chemical composition engineering due to its ternary structure (PEA^+, Sn^{2+}, and I^-). It has been reported that a redshift of the light absorption of such 2D perovskite can be achieved by partially replacing PEA^+ by formamidinium (FA^+).[29] Figure S8 of the Supporting Information shows a blueshift of the absorption of our synthesized $(PEA)_2SnI_4$, in which I^- is partially replaced by Br^-. These results demonstrate that wavelength selectivity can be achieved by adjusting the
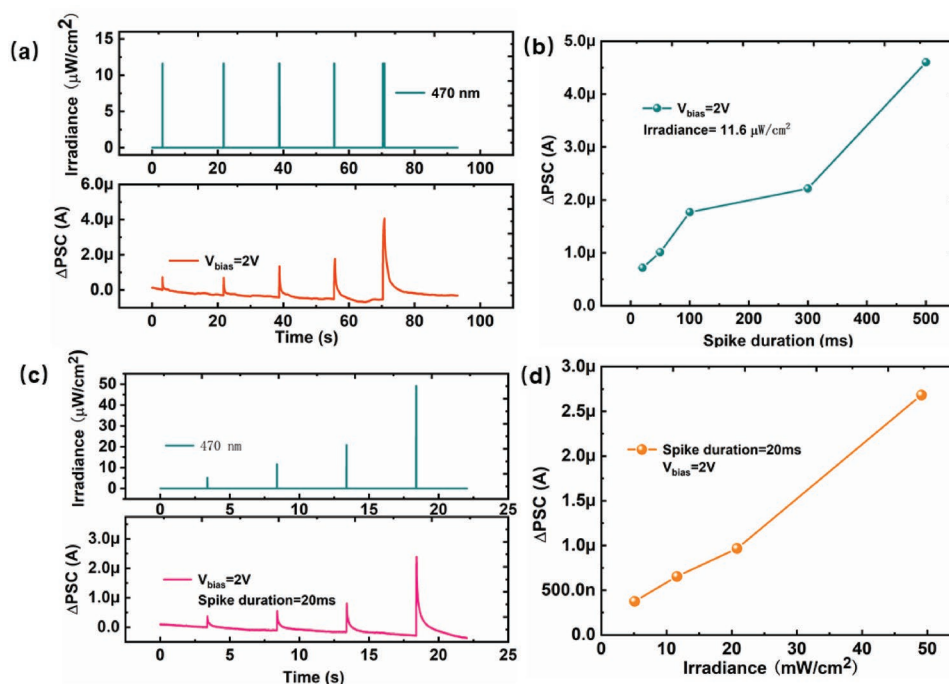
Figure 3. a) The ΔPSC response to a train of light spikes with the same light irradiance and duration times ranging from 20 to 500 ms. b) The ΔPSC plotted as a function of the spike duration. c) The ΔPSC response to a train of light spikes with the same duration time and irradiances ranging from 5.1 to 49.1 μW cm^{-2}. d) The ΔPSC plotted as a function of the light irradiance.

composition of 2D perovskite, which has not been reported in other photoelectric materials. In this way, the synaptic function can be modulated by changing its composition, indicating a method to achieve multifunctional artificial synapses. In the following part, we will discuss the origin and characteristics of the LTP based on Sn vacancy-modulated photomemory effect.

Here, we investigate the time response of our synaptic devices by applying different numbers of light spikes (duration time of 20 ms and internal time of 30 ms) ranging from 100 to 1000 to emulate the LTP. **Figure 4**a shows the normalized PSC after repeated light stimulations, indicating an enhanced memory effect with the increase in the number of light spikes. In state-of-art artificial synaptic devices, device conductivity is widely treated as synaptic weight.[41] Here, the relative change of synaptic weight (ΔW) is defined as $(I_2-I_1)/I_1$, where I_1 and I_2 represent the PSCs measured before and 5 s after the train of light spikes is applied as shown in the inset of Figure 4b. It can be seen that the ΔW increases with the increase in number of light spikes and shows little change for spike numbers above 800. By applying repeated light stimulations, the STP to LTP transition has been achieved in our synaptic devices. To gain deeper insight into the memory effect of 2D perovskite, a long duration light source is applied to investigate the PSC decay characteristics. As shown in Figure 4c, the photoresponse identified as $(I_L-I_D)/I_D$, where I_L represents the PSC under illumination and I_D represents the PSC in the dark, exhibits a similar rise time but an increasing decay time with the light duration increasing from 1 to 20 s. A long sustained current after removing the illumination, known as persistent photocurrent (PPC), is observed, which contributes to a photomemory effect. To illustrate the

photocurrent decay in the absence of illumination, a temporal model with two exponential terms is used to fit the decay curves under the illumination with the light duration of 10 s shown in Figure 4d. It can be clearly seen that there is a shorter time constant ($t_1 \approx 2.67$ s) and a longer time constant ($t_2 \approx 268.02$ s). To further address this phenomenon, both time constants t_1 and t_2 are plotted as a function of the light duration as shown in Figure 4e, and both exhibit the increasing trend with the extension of the illuminating time. The shorter time constant t_1 increases from 1.28 to 2.87 s and the longer time constant t_2 increases from 42.3 to 285.15 s and becomes saturated when the light duration is longer than 10 s.

We attribute these two time constants of the photocurrent decay to relaxations of two types of trapping states. When the light is switched off, the channel current will be reduced due to the recombination of photogenerated carriers. In this process, traps in the channel or the interface play an important role in the current decay. Based on the fitting results, we attribute the shorter decay component t_1 to the shallower traps, with which the trapped carriers can be released completely, and the longer decay component t_2 to the deeper traps, which can hold the carriers for longer time. This model can explain the coexistence of STP and LTP as discussed earlier. For STP, the spike duration is much shorter and the recombination of photogenerated carriers is dominated by the carrier release from the shallower traps because the deeper traps may require longer light exposure to be filled. As shown in Figure 1, the channel conductance can quickly return to its original state due to a shorter trapping/detrapping process caused by the shallower traps. When the light exposure is strong enough, the photogenerated carriers may be trapped by the deeper traps and cause the
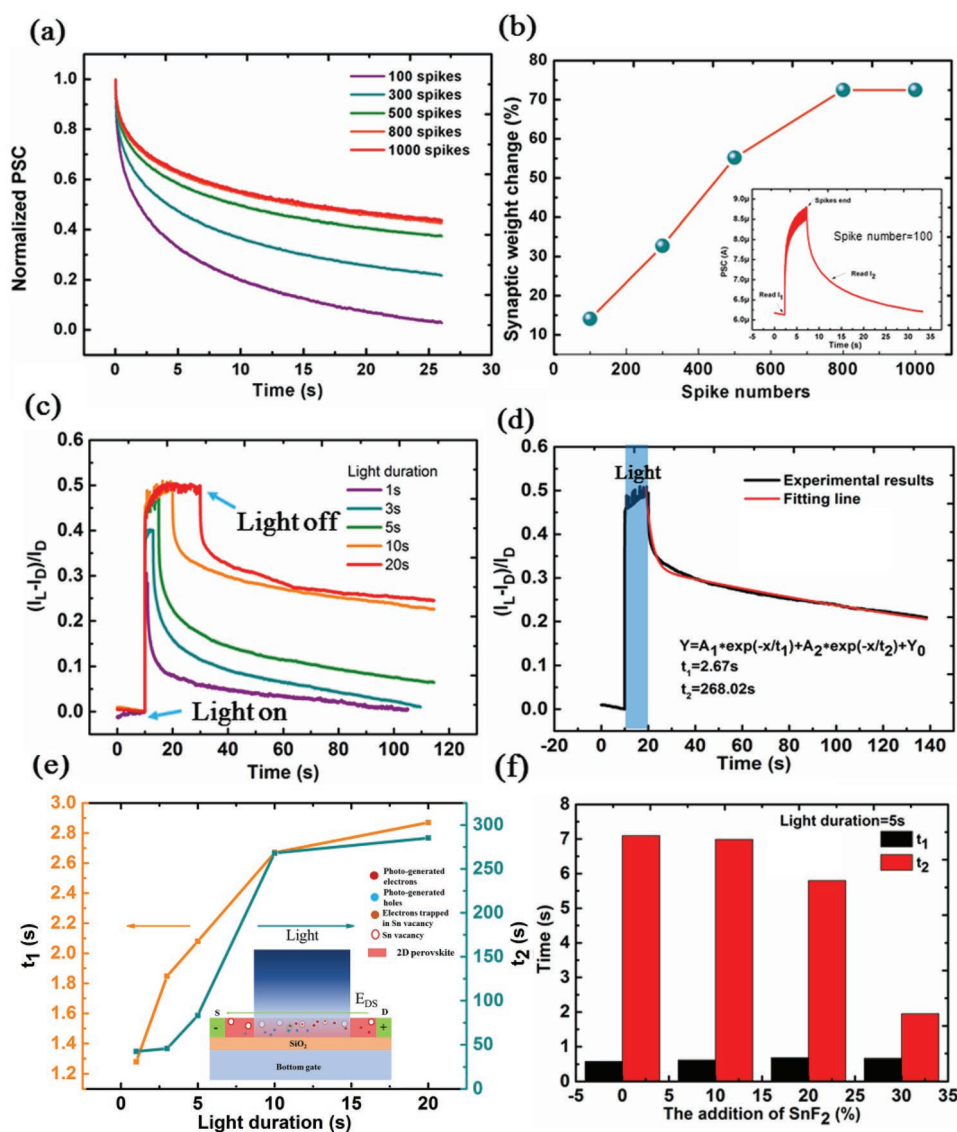
Figure 4. a) Normalized PSC decay characteristics after different numbers of light spikes ranging from 100 to 1000. b) The synaptic weight change plotted against light spike numbers. The inset is the PSC stimulated by 100 light spikes. c) The temporal response of our devices with light durations ranging from 1 to 20 s. d) The fitting result of the photocurrent decay by a temporal model with two exponential terms under a light duration of 10 s. e) The time constants t_1 and t_2 are plotted as a function of the light duration. The inset is a schematic illustration of the charge trapping process induced by Sn vacancies in the $(PEA)_2SnI_4$ channel. f) The time constants t_1 and t_2 are plotted as a function of the concentration of the added SnF_2.

stronger photogating (PG) effect and longer detrapping time. When removing the light, the channel conductance first rapidly decreases and then becomes stable because two different time constants dominate this process at different time scale. In particular, the deep-trapped electrons, which may not be released, may continuously induce the holes by the PG effect, resulting in the photomemory characteristics shown in Figure S9 (Supporting Information). In addition, the PSC curve triggered by just a single spike with duration of 20 ms is also fitted by a temporal model with two exponential terms (Figure S10, Supporting Information). The time constants t_1 and t_2 are calculated to be 0.30 and 0.02 s, respectively, which confirms different contributions of different trapping states to STP and LTP.

Although these trapping mechanisms have been widely investigated,[42–44] the origin of traps is still under debate. The shallower traps are often attributed to the uncompensated dangling bonds or the structural defects in synthesized 2D layered materials such as MoS_2 as well as the vacancy defects generated by halide ions such as I^-.[45–48] These traps can originate from both the external environment and intrinsic defects of materials. Here, we only focus on the deeper traps, which may be more important to achieve the memory effect of artificial synapses. Sn vacancies have been found to be responsible for the deeper traps because Sn^{2+} is easily oxidized to Sn^{4+}.[49] The positive Sn vacancies may capture the photogenerated electrons and cause the PG effect to induce more holes, modulating the channel conductance and this physical process has

been illustrated in the inset of Figure 4e. To confirm the effect of Sn vacancies on the longer trapping/detrapping process, we introduce SnF_2, which can relieve the oxidation process of Sn^{2+} and suppress the generation of Sn vacancies.[50] As shown in Figure 4f, t_1 and t_2 have been extracted by fitting the time response curves under illumination for 5 s. It is observed that t_1 changes little but t_2 dramatically decreases when the concentration of the added SnF_2 reaches 30 mol%, indicating the suppression of the PG effect caused by the decrease of Sn vacancies. To further demonstrate the origin of Sn vacancies, X-ray photoelectron spectroscopy was used to confirm the decrease of Sn vacancies caused by the introduction of SnF_2 as shown in Figure S11 (Supporting Information). The result shows that the perovskite films with 30 mol% SnF_2 exhibited a much lower amount of Sn^{4+} than pristine perovskite film. The Sn chemical potential is increased by the addition of SnF_2, which inhibits the formation of Sn vacancies.[51] In this way, the performance of our artificial synapses based on $(PEA)_2SnI_4$ can be effectively modulated by the density of Sn vacancies.

3. Conclusion

In summary, we have demonstrated a novel light-stimulated synaptic photoconductor based on 2D perovskite ($(PEA)_2SnI_4$). Synaptic plasticity including paired-pulse facilitation, and the transition from short-term to long-term were successfully mimicked. The strong dependence of the PSC on the light spike duration, frequency, irradiance, and wavelength indicates an efficient way to modulate the connection strength between presynapse and postsynapse. The long-term synaptic plasticity has been preliminarily achieved through repeated light spikes. By analyzing the memory behaviors of channel current under the illumination with long duration, two trapping mechanisms have been found to be responsible for this behavior and Sn-vacancy dominant LTP can be modulated by controlling the proportion of Sn^{4+}. The electrical and optical performances of 2D perovskite can be easily modulated by chemical engineering such as through composition control, which can open up a new platform to satisfy the complexity and freedoms required by neuromorphic computing and hopefully enable the next-generation of artificial photonics-enabled neural networks.

4. Experimental Section

Synthesis: Phenylethylammonium iodine (PEAI) prepared according to a previous report[21] was mixed with SnI_2 (Acros, 99.999%) at a mole ratio of 2:1, dissolved in N,N-dimethylformamide (Acros, 99.9%) at a concentration of 0.3 mol L^{-1}, and stirred for at least 3 h in a glovebox filled with argon.

Device Fabrication: A highly p-doped Si wafer with a 90-nm thick SiO_2 layer was used as the bottom-gated substrate. Source/drain electrodes composed of 50 nm thick Au and 10 nm thick Cr were defined by photolithography and deposited through electron beam evaporation followed by a lift-off process. Then, the as-fabricated substrate was treated by a 15 min UV-ozone and transferred to a glovebox filled with argon gas. The $(PEA)_2SnI_4$ precursor was spin-coated on the as-fabricated substrate. The $(PEA)_2SnI_4$ prepared by a facile one-step solution processing strategy serves as the functional channel sensitive to the light stimuli.

Characterizations: The UV–vis spectrum was measured with a Lambda 35 UV–vis spectrometer (PerkinElmer). The X-ray diffraction (XRD) patterns were carried out on a Bruker D8 ADVANCE diffractometer with Cu Kα ($\lambda = 1.5406$ Å) radiation. The electrical measurements were performed on an Agilent 1500 semiconductor characterization system. The light-stimuli with different irradiance powers were generated by a light-emitting diode (LED) modulated by a Keithley 2614B digital source meter. All the measurements were performed in air at room temperature.

Supporting Information

Supporting Information is available from the Wiley Online Library or from the author.

Conflict of Interest

The authors declare no conflict of interest.

[1] P. Gkoupidenis, N. Schaefer, B. Garlan, G. G. Malliaras, *Adv. Mater.* **2015**, *27*, 7176.
[2] R. Yang, K. Terabe, Y. Yao, T. Tsuruoka, T. Hasegawa, J. K. Gimzewski, M. Aono, *Nanotechnology* **2013**, *24*, 384003.
[3] L. Q. Zhu, C. J. Wan, L. Q. Guo, Y. Shi, Q. Wan, *Nat. Commun.* **2014**, *5*, 3158.
[4] C. Sherrington, *The Integrative Action of the Nervous System*, CUP Archive, Cambridge, **1952**.
[5] G.-q. Bi, M.-m. Poo, *J. Neurosci.* **1998**, *18*, 10464.
[6] T. Chang, S.-H. Jo, W. Lu, *ACS Nano* **2011**, *5*, 7669.
[7] P. Balakrishna Pillai, M. M. De Souza, *ACS Appl. Mater. Interfaces* **2017**, *9*, 1609.
[8] K. Kim, C. L. Chen, Q. Truong, A. M. Shen, Y. Chen, *Adv. Mater.* **2013**, *25*, 1693.
[9] H. Tian, W. Mi, X.-F. Wang, H. Zhao, Q.-Y. Xie, C. Li, Y.-X. Li, Y. Yang, T.-L. Ren, *Nano Lett.* **2015**, *15*, 8013.
[10] W. Xu, S.-Y. Min, H. Hwang, T.-W. Lee, *Sci. Adv.* **2016**, *2*, e1501326.
[11] Y. van de Burgt, E. Lubberman, E. J. Fuller, S. T. Keene, G. C. Faria, S. Agarwal, M. J. Marinella, A. A. Talin, A. Salleo, *Nat. Mater.* **2017**, *16*, 414.

[12] P. Gkoupidenis, D. A. Koutsouras, G. G. Malliaras, *Nat. Commun.* **2017**, *8*, 15448.

[13] S. Cassenaer, G. Laurent, *Nature* **2012**, *482*, 47.

[14] W.-C. A. Lee, V. Bonin, M. Reed, B. J. Graham, G. Hood, K. Glattfelder, R. C. Reid, *Nature* **2016**, *532*, 370.

[15] S. Qin, F. Wang, Y. Liu, Q. Wan, X. Wang, Y. Xu, Y. Shi, X. Wang, R. Zhang, *2D Mater.* **2017**, *4*, 035022.

[16] A. Destexhe, E. Marder, *Nature* **2004**, *431*, 789.

[17] M. Lee, W. Lee, S. Choi, J. W. Jo, J. Kim, S. K. Park, Y. H. Kim, *Adv. Mater.* **2017**, *29*, 1700951.

[18] H. K. Li, T. P. Chen, P. Liu, S. Hu, Y. Liu, Q. Zhang, P. S. Lee, *J. Appl. Phys.* **2016**, *119*, 244505.

[19] D. Rosenbluth, K. Kravtsov, M. P. Fok, P. R. Prucnal, *Opt. Express* **2009**, *17*, 22767.

[20] H. Tan, Z. Ni, W. Peng, S. Du, X. Liu, S. Zhao, W. Li, Z. Ye, M. Xu, Y. Xu, X. Pi, D. Yang, *Nano Energy* **2018**, *52*, 422.

[21] Y. Wang, Z. Lv, J. Chen, Z. Wang, Y. Zhou, L. Zhou, X. Chen, S. Han, *Adv. Mater.* **2018**, *30*, 1802883.

[22] M. A. Green, A. Ho-Baillie, H. J. Snaith, *Nat. Photonics* **2014**, *8*, 506.

[23] P. Gao, M. Grätzel, M. K. Nazeeruddin, *Energy Environ. Sci.* **2014**, *7*, 2448.

[24] M. M. Lee, J. Teuscher, T. Miyasaka, T. N. Murakami, H. J. Snaith, *Science* **2012**, *338*, 643.

[25] Z.-K. Tan, R. S. Moghaddam, M. L. Lai, P. Docampo, R. Higler, F. Deschler, M. Price, A. Sadhanala, L. M. Pazos, D. Credgington, *Nat. Nanotechnol.* **2014**, *9*, 687.

[26] Y. Lee, J. Kwon, E. Hwang, C. H. Ra, W. J. Yoo, J. H. Ahn, J. H. Park, J. H. Cho, *Adv. Mater.* **2015**, *27*, 41.

[27] W. Xu, H. Cho, Y. H. Kim, Y. T. Kim, C. Wolf, C. G. Park, T. W. Lee, *Adv. Mater.* **2016**, *28*, 5916.

[28] C. Chen, X. Zhang, G. Wu, H. Li, H. Chen, *Adv. Opt. Mater.* **2017**, *5*, 1600539.

[29] Y. Liao, H. Liu, W. Zhou, D. Yang, Y. Shang, Z. Shi, B. Li, X. Jiang, L. Zhang, L. N. Quan, *J. Am. Chem. Soc.* **2017**, *139*, 6693.

[30] A. Waleed, M. M. Tavakoli, L. Gu, Z. Wang, D. Zhang, A. Manikandan, Q. Zhang, R. Zhang, Y.-L. Chueh, Z. Fan, *Nano Lett.* **2017**, *17*, 523.

[31] I. Chung, J.-H. Song, J. Im, J. Androulakis, C. D. Malliakas, H. Li, A. J. Freeman, J. T. Kenney, M. G. Kanatzidis, *J. Am. Chem. Soc.* **2012**, *134*, 8579.

[32] H. K. He, R. Yang, W. Zhou, H. M. Huang, J. Xiong, L. Gan, T. Y. Zhai, X. Guo, *Small* **2018**, *14*, 1800079.

[33] R. S. Zucker, W. G. Regehr, *Annu. Rev. Physiol.* **2002**, *64*, 355.

[34] D. V. Buonomano, *J. Neurosci.* **2000**, *20*, 1129.

[35] T. Ohno, T. Hasegawa, T. Tsuruoka, K. Terabe, J. K. Gimzewski, M. Aono, *Nat. Mater.* **2011**, *10*, 591.

[36] J. L. McGaugh, *Science* **2000**, *287*, 248.

[37] L. Abbott, W. G. Regehr, *Nature* **2004**, *431*, 796.

[38] C. J. Wan, Y. H. Liu, L. Q. Zhu, P. Feng, Y. Shi, Q. Wan, *ACS Appl. Mater. Interfaces* **2016**, *8*, 9762.

[39] R. Shapley, M. Hawken, D. L. Ringach, *Neuron* **2003**, *38*, 689.

[40] J. Lee, S. Pak, Y.-W. Lee, Y. Cho, J. Hong, P. Giraud, H. S. Shin, S. M. Morris, J. I. Sohn, S. Cha, *Nat. Commun.* **2017**, *8*, 14734.

[41] Z. Q. Wang, H. Y. Xu, X. H. Li, H. Yu, Y. C. Liu, X. J. Zhu, *Adv. Funct. Mater.* **2012**, *22*, 2759.

[42] W. Zhang, J. K. Huang, C. H. Chen, Y. H. Chang, Y. J. Cheng, L. J. Li, *Adv. Mater.* **2013**, *25*, 3456.

[43] H. Fang, W. Hu, *Adv. Sci.* **2017**, *4*, 1700323.

[44] A. Di Bartolomeo, L. Genovese, T. Foller, F. Giubileo, G. Luongo, L. Croin, S.-J. Liang, L. Ang, M. Schleberger, *Nanotechnology* **2017**, *28*, 214002.

[45] S. Ghatak, A. Ghosh, *Appl. Phys. Lett.* **2013**, *103*, 122103.

[46] Z. Lin, B. R. Carvalho, E. Kahn, R. Lv, R. Rao, H. Terrones, M. A. Pimenta, M. Terrones, *2D Mater.* **2016**, *3*, 022002.

[47] C. Eames, J. M. Frost, P. R. Barnes, B. C. O'regan, A. Walsh, M. S. Islam, *Nat. Commun.* **2015**, *6*, 7497.

[48] W. J. Yin, T. Shi, Y. Yan, *Appl. Phys. Lett.* **2014**, *104*, 063903.

[49] T. Yokoyama, D. H. Cao, C. C. Stoumpos, T.-B. Song, Y. Sato, S. Aramaki, M. G. Kanatzidis, *J. Phys. Chem. Lett.* **2016**, *7*, 776.

[50] M. H. Kumar, S. Dharani, W. L. Leong, P. P. Boix, R. R. Prabhakar, T. Baikie, C. Shi, H. Ding, R. Ramesh, M. Asta, *Adv. Mater.* **2014**, *26*, 7122.

[51] L. Qian, Y. Sun, M. Wu, C. Li, D. Xie, L. Ding, G. Shi, *Nanoscale* **2018**, *10*, 6837.